PHYSICAL REVIEW D **92,** 105011 (2015)

Shear viscosity of the Φ^4 theory from classical simulation

M. M. Homor[*] and A. Jakovac[†]

Institute of Physics, Eotvos University, Pazmany Peter setany 1/A, Budapest H-1117, Hungary

(Received 4 June 2015; published 6 November 2015)

Shear viscosity of the classical Φ^4 theory is measured using classical microcanonical simulation. To calculate the Kubo formula, we measure the energy-momentum tensor correlation function and apply the Green-Kubo relation. Given that this is a classical theory, the results depend on the cutoff, which should be chosen in the range of the temperature. Comparison with experimentally accessible systems is also performed.

DOI: 10.1103/PhysRevD.92.105011 PACS numbers: 11.10.Wx, 05.60.Gg, 11.10.Lm, 51.20.+d

I. INTRODUCTION

Transport coefficients, in particular shear viscosity, are not easily accessible quantities in perturbative quantum field theory calculations. Transport is a characteristic of systems in which information is spread by diffusion. The time evolution is $\sim\sqrt{Dt}$, the diffusion constant being the corresponding transport coefficient. The diffusion constant itself is proportional to the quasiparticle lifetime $D \sim \tau$. This is infinite in a free gas, and inversely proportional to some powers of the coupling constant for weak couplings. Therefore the perturbative evaluation of the Kubo formula [1] requires resummation of an infinite set of diagrams [2]. To circumvent this difficulty one can use effective methods to calculate the transport coefficients. One of these methods is the use of Boltzmann equations, which is equivalent to the resummation of the singular part of the full perturbation series [3,4]. The Boltzmann equation method is used to obtain general results in gauge theories [5,6], proving that to the leading order one has a shear viscosity $\eta \sim \frac{1}{g^4 \ln g^{-1}}$. Boltzmann equation methods are used also in other models to compute shear viscosity, like in meson models [7–9] or in full QCD [10,11]. Other perturbation theory motivated methods to calculate the shear viscosity are 2-particle-irreducible resummation techniques [12] or the generalized quasiparticle approach [13].

Apart from the technical difficulties, the applicability of perturbation theory also makes these results less relevant for strongly interacting QCD-like systems. The small value of the shear viscosity of the QCD plasma, reported by analyses of experimental data [14], suggests that the QCD matter is close to a perfect liquid [15]. This implies that the interaction is rather strong, the quasiparticle lifetime is very short, and so perturbation theory is hardly applicable.

Where perturbation theory is not well applicable, one seeks nonperturbative methods. Computer Monte Carlo (MC) simulation of QCD was used to extract shear viscosity data roughly in agreement with measurements [16]. The temporal range of the Euclidean formalism of the MC setup, however, makes the correlations less sensitive to long range physics, which are relevant for transport [17]. Another popular method is to use the dual theory approach, based on AdS/CFT correspondence. Then weakly coupled five-dimensional gravity can be used to compute transport coefficients in strongly coupled (conformal) field theories [18,19]. There are several model studies in this field which calculate shear viscosity by this method.

Another nonperturbative method to approach the dynamics of quantum field theory is the use of classical theories to study both equilibrium [20–27] and nonequilibrium phenomena [28–36]. Here one applies classical equations of motion starting from some initial conditions, and solve them by numerical methods on a finite mesh. The system thermalizes,[1] which in a classical system means equipartition of the energy. From the classical trajectories we can evaluate expectation values of different observables as time averages.

From the point of view of perturbation theory, classical and quantum systems are similar [22]. In particular one can study expectation values of composite operators like $\langle\Phi^2(x)\Phi^2(y)\rangle$. Comparing the classical and quantum computations, one finds that with an appropriate choice of the cutoff of the classical theory $\Lambda_{\rm cl} \sim T$, the quantum results can be nicely reproduced [37].

Encouraged by these results, we tried to use classical simulations to compute the shear viscosity in a simple bosonic classical system, the Φ^4 model. Our strategy follows the general setup of the earlier studies (cf. for example [28]): we start from an initial condition and let the system evolve in time. We eventually use stochastic terms to speed up the thermalization, but only for technical reasons, and just for a short period of time (for details, cf. Sec. III.) After we reach thermal equilibrium (which is monitored carefully), we start measurements. The Kubo formula for the shear viscosity [1]

[*]homor.marietta.m@gmail.com
[†]jakovac@caesar.elte.hu

[1]Note that we work with finite systems with finite energy density where thermalization is possible.

contains the commutator of spatial components of the energy-momentum tensor. We computed it with the help of the Green-Kubo relation which is the classical counterpart of the quantum Kubo-Martin-Schwinger relation (fluctuation dissipation theorem) [38]. This system has the potential to show a phase transition, similarly to the QCD case (although it is a second order here, as opposed to the crossover nature in QCD). This makes it possible to study the η/s ratio near the phase transition.

The paper is organized as follows. First we give an overview of the details of the discretization and classical simulation method for the Φ^4 model in Sec. II. In Sec. III we discuss the thermalization process and the measured characteristics of the thermal equilibrium, in particular thermal mass. In Sec. IV we report on our results of the energy-momentum tensor correlation functions and the classical values of the shear viscosity. In Sec. V we apply our method to quantum systems and present the η/s ratio, also in comparison with the experimentally measured values in different systems. The paper is closed with a Summary.

II. THE SYSTEM: DISCRETIZATION AND SIMULATION ALGORITHM

The system we study is the quartic scalar model, which has the Hamiltonian density

$$\mathcal{H}_{\mathbf{x}} = \frac{1}{2}\Pi^2(\mathbf{x}) + \frac{1}{2}(\nabla\Phi(\mathbf{x}))^2 + \frac{m^2}{2}\Phi^2(\mathbf{x}) + \frac{\lambda}{24}\Phi^4(\mathbf{x}). \tag{1}$$

Here Φ denotes the field and Π its canonical conjugate. The corresponding equations of motion (EoM) are

$$\dot{\Phi} = \Pi, \qquad \dot{\Pi} = \Delta\Phi - m^2\Phi - \frac{\lambda}{6}\Phi^3. \tag{2}$$

We remark that by rescaling the fields $\Phi \to \Phi/\sqrt{\lambda}$ and $\Pi \to \Pi/\sqrt{\lambda}$, the equations of motion become λ-independent. We could work therefore with $\lambda = 1$, but for better readability we keep the notation of λ.

We discretize the model on a symmetric finite spacelike mesh,

$$U = \left\{ \mathbf{x} = \sum_{i=1}^{3} n_i a \mathbf{e}_i | n_i = 0 \ldots N-1 \right\},$$

where $\mathbf{e}_i$ are orthogonal unit vectors and a is the lattice spacing; we express all dimensional quantities in lattice units and so we choose $a = 1$. For the lattice size we have in our simulations $N = 36$, 40, and 50, and we use periodic boundary conditions. The discretized Laplacian is

$$\Delta\Phi(\mathbf{x}) = \sum_{i=1}^{3} [\Phi(\mathbf{x}+\mathbf{e}_i) - 2\Phi(\mathbf{x}) + \Phi(\mathbf{x}-\mathbf{e}_i)].$$

The discretized Hamiltonian can be written as $H = \sum_{\mathbf{x}\in U}\mathcal{H}_{\mathbf{x}}$, where the Hamiltonian density is formally equivalent to (1), with $(\nabla\Phi(\mathbf{x}))^2 = \sum_{i=1}^{3}[\Phi(\mathbf{x}+\mathbf{e}_i) - \Phi(\mathbf{x})]^2$. This is, however, not a local expression anymore, as it connects nearest-neighbor field values.

For the evaluation of expectation values we also need Fourier transformation. It is defined on the reciprocal lattice $\bar{U}$ with the following definition (which corresponds to the `fftw++` conventions [39]):

$$f_{\mathbf{k}\in\bar{U}} = \sum_{\mathbf{x}\in U} \exp^{-2\pi i(\mathbf{kx})/N} f_{\mathbf{x}},$$
$$f_{\mathbf{x}\in U} = \frac{1}{N^3}\sum_{\mathbf{k}\in\bar{U}} \exp^{2\pi i(\mathbf{kx})/N} f_{\mathbf{k}}. \tag{3}$$

The reciprocal lattice is equivalent with the original lattice in the case of the cubic lattices we used. The Fourier-transformed Hamiltonian reads

$$H = \frac{1}{N^3}\sum_{\mathbf{k}\in\bar{U}}\left[\frac{1}{2}|\Pi_{\mathbf{k}}|^2 + \frac{1}{2}\omega_k^2|\Phi_{\mathbf{k}}|^2\right] + \frac{\lambda}{24N^6}\sum_{\mathbf{k}_i\in\bar{U}}\Phi_{\mathbf{k}_1}\Phi_{\mathbf{k}_2}\Phi_{\mathbf{k}_3}\Phi_{\mathbf{k}_4}, \tag{4}$$

where $\omega_k^2 = m^2 + \sum_{i=1}^{3} 4\sin^2(\frac{\pi\mathbf{k}\mathbf{e}_i}{N})$, and $\sum_i \mathbf{k}_i = 0$ in the last term.

The time evolution in the computer is realized using the leap-frog algorithm. Here one chooses a time step dt, so at the nth step one arrives at time $t = ndt$. In the time step from $n-1$ to n, the two equations of (2) are treated subsequently: first one evolves the field configuration

$$\Phi^{(n)}(\mathbf{x}) = \Phi^{(n-1)} + dt\Pi^{(n-1)}(\mathbf{x}), \tag{5}$$

and then the canonically conjugated field configuration, using the new values of the field:

$$\Pi^{(n)}(\mathbf{x}) = \Pi^{(n-1)}(\mathbf{x}) + dt\left(\Delta\Phi^{(n)}(\mathbf{x}) - m^2\Phi^{(n)}(\mathbf{x}) - \frac{\lambda}{6}(\Phi^{(n)}(\mathbf{x}))^3\right), \tag{6}$$

with the discretized Laplacian.

We can use the notion of the energy in the discretized model, too, as $E = H = \sum_{\mathbf{x}\in U}\mathcal{H}$. This quantity is conserved only for continuous time evolution; since we evolve the time in discrete steps, the total energy is not necessarily conserved. An important consistency check for the reliability of the algorithm is that in the long run the energy remains conserved, as it can be seen in Fig. 1. The leap-frog algorithm satisfies this requirement.

The classical ground state of the system, i.e., the minimum of the energy, is at a spatially homogeneous

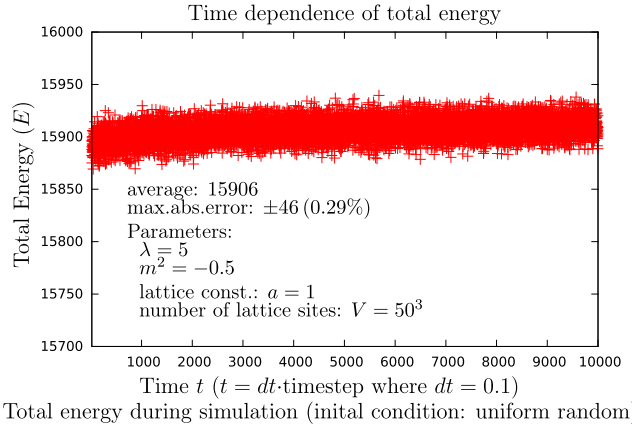

FIG. 1 (color online). The total energy as a function of time. In the leap-frog algorithm, the total energy remains stable.

field. If m^2 and λ are positive, then the minimum is reached at $\Phi = \Pi = 0$. The coupling λ must be positive; otherwise, the Hamiltonian of the system is not bounded from below. If $m^2 < 0$, the minimal energy is reached at a finite $|\Phi| = \Phi_0$ value: this is the spontaneous symmetry breaking (SSB) phase. The minimum condition yields $\Phi_0^2 = \frac{-6m^2}{\lambda}$.

III. DESCRIPTION OF THE THERMAL EQUILIBRIUM

Since we are primarily interested in the equilibrium properties of the system, we may start from an arbitrary initial condition. Practically we started with $\Phi(\mathbf{x}) \equiv 0$ and from random values of $\Pi(\mathbf{x})$. After a certain time evolution (practically around $t/a \sim 10000$), we arrive at a steady equilibrium state. While the complete system forms a microcanonical ensemble, for local observables we can use a canonical ensemble. To determine its properties, we have taken the histogram of $\Pi_{\mathbf{x}}$, and found that it can be described by a Gaussian. This corresponds to the Boltzmann distribution $\sim e^{-\beta\Pi_x^2}$, with β as a parameter interpreted as the "inverse temperature." Therefore one can compute the expectation value of a local operator $A(\Phi, \Pi)$, which depends on the fields as

$$\langle A(\Phi,\Pi)\rangle = \frac{1}{Z}\int \prod_{x\in U} d\Phi_x d\Pi_x A(\Phi,\Pi) e^{-\beta H(\Phi,\Pi)}, \quad (7)$$

where $Z = \int \prod_{x\in U} d\Phi_x d\Pi_x e^{-\beta H(\Phi,\Pi)}$. In Fourier space we should handle the problem that there is a relation between the integration variables $\Phi_{\mathbf{k}} = \Phi^*_{-\mathbf{k}}$, and similarly for $\Pi_{\mathbf{k}}$, because Φ and Π are real in coordinate space. To overcome this problem we must cut the Fourier space into two parts and apply the path integral over configurations living only on just half of it. For the real part we use the $k_3 \geq 0$ part and for the imaginary part the $k_3 < 0$ part (the $k_3 = 0$ plane is a null-measure set). Therefore we can use a purely real field:

$$\tilde{\Phi}_{\mathbf{k}} = \begin{cases} \mathrm{Re}\Phi_{\mathbf{k}} & \text{if } k_3 \geq 0 \\ \mathrm{Im}\Phi_{\mathbf{k}} & \text{if } k_3 < 0. \end{cases} \quad (8)$$

This allows us to write

$$\langle A(\Phi,\Pi)\rangle = \frac{1}{Z}\int \prod_{\mathbf{k}\in\bar{U}} d\tilde{\Pi}_{\mathbf{k}} d\tilde{\Phi}_{\mathbf{k}} A(\Phi,\Pi) e^{-\beta H(\Phi,\Pi)}. \quad (9)$$

To measure the temperature we use the relation

$$\langle |\Pi_{\mathbf{k}}|^2\rangle = \frac{1}{\tilde{Z}_{\mathbf{k}}}\int_{-\infty}^{\infty} d\tilde{\Pi}_{\mathbf{k}} (\tilde{\Pi}_{\mathbf{k}}^2 + \tilde{\Pi}_{-\mathbf{k}}^2) e^{-\beta\frac{1}{2N^3}(\tilde{\Pi}_{\mathbf{k}}^2 + \tilde{\Pi}_{-\mathbf{k}}^2)} = 2N^3 T, \quad (10)$$

with $T = 1/\beta$. Using this formula we can check that the system arrived at equilibrium by verifying that $\langle |\Pi_{\mathbf{k}}|^2\rangle$ is independent of $\mathbf{k}$ (equipartition). An example of this distribution in a completely thermalized state is shown in Fig. 2.

We remark that the above canonical equilibrium description is in fact a 3D field theory of the initial conditions. As compared to the original action which is four dimensional, we have a dimensionally reduced theory. As a consequence the mass (energy) dimension of the field is $[\Phi] = 1/2$. This fact will be used later when we apply dimensional analysis.

In the thermal equilibrium we can perform perturbation theory. Although at large coupling (where we actually performed our simulations) results of perturbation theory are not necessarily perfect, but in several aspects these may "guide the eye" to understand some robust features of the results. The details of perturbation theory in the classical theory can be found in [22]. One uses here two types of propagators,

$$G_{\mathrm{ret}}(k) = \frac{1}{(k_0 + i\varepsilon)^2 - \omega_k^2}, \qquad iG_{3D}(k) = \frac{T}{k_0}\varrho(k), \quad (11)$$

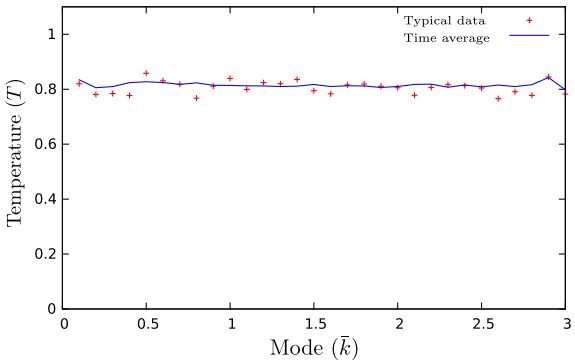

FIG. 2 (color online). Mode dependence of temperature [$\bar{k}^2 = \sum_{i=1}^{3} \sin^2(2\pi \frac{\mathbf{k}\mathbf{e}_i}{N})$].

where the free spectral function is

$$\varrho(k) = 2\pi \mathrm{sgn}(k_0)\delta(k_0^2 - \omega_k^2), \tag{12}$$

and

$$\omega_k^2 = \sum_{i=1}^{3} 4\sin^2\left(\frac{\pi k_i}{N}\right) + m^2, \qquad k_i \in 0 \ldots N-1. \tag{13}$$

As a final, technical issue, we remark that solving the field equation corresponds to the pure microcanonical, energy conserving approach to the thermodynamics. However, knowing that the system reaches equilibrium with Boltzmann distribution, we can also use a canonical approach with a heat bath: in the language of the equations of motion it can be realized as a Langevin equation. There we introduce a γ damping parameter and a noise represented by $\xi(\mathbf{x})$ independent stochastic variables with uniform distribution at each time step. We then change the update of Π to

$$\Pi^{(n)}(\mathbf{x}) = (1-\gamma dt)\Pi^{(n-1)}(\mathbf{x}) + dt\Big(\Delta\Phi^{(n)}(\mathbf{x}) - m^2\Phi^{(n)}(\mathbf{x}) - \frac{\lambda}{6}(\Phi^{(n)}(\mathbf{x}))^3 + \xi(\mathbf{x})\Big). \tag{14}$$

This stochastic process drives the system towards an equilibrium distribution with $\mathcal{P}(E) \sim e^{-\beta E}$ distribution function. Because of the Einstein relation $2\gamma T = \langle \xi\xi \rangle$ we can control the temperature of the thermal distribution. This algorithm can largely speed up the thermalization. After the system arrives at equilibrium, we switch off the noise and damping terms so that they do not influence the measurements.

IV. EQUILIBRIUM OBSERVABLES

After we reach the equilibrium state, we can measure expectation values using the time average:

$$\langle A(\Phi,\Pi)\rangle = \frac{1}{t}\int_{t_0}^{t_0+t} dt' A(\Phi(t),\Pi(t)). \tag{15}$$

The equilibrium system can be characterized by a single value, for example, the temperature.

A. Energy

We measured the relation between the temperature and the energy density; the results are shown in Fig. 3. We found that the relation is linear, with slightly different slope in the symmetric and SSB regimes. One can clearly identify the phase transition region. Since our goal was not to study the phase transition point very accurately, we did not try to focus on this regime close enough to be able to tell details about it.

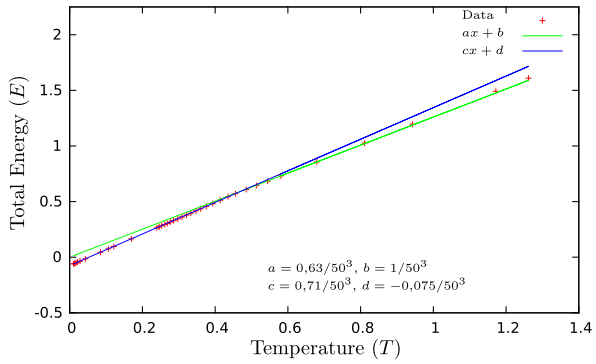

FIG. 3 (color online). Temperature dependence of total energy ($N^3 = V = 50^3$), $\lambda = 5$, $m^2 = -0.5$.

This figure tells us that the heat capacity is proportional to the number of modes, as it is expected from a classical theory. Rewriting the lattice spacing a, this also means that the specific heat is proportional to a^3. This is the well-known Rayleigh instability (ultraviolet catastrophe) of the classical plasma. To have a physically meaningful result, the lattice spacing must have a finite value.

B. Mass and symmetry breaking

It is important to note that the mass parameter of the Lagrangian (the bare mass) is not the same as the mass appearing in the observables (the effective mass). Physically it happens because of the nontrivial effect of the fluctuations.

To estimate this effect (cf. Refs. [28,29]) we used the background field method. We shifted the classical field with its expectation value: $\Phi \to \Phi_0 + \varphi$, where $\langle\varphi\rangle = 0$. The shifted Lagrangian reads

$$\mathcal{L} = -\frac{m^2}{2}\bar{\Phi}^2 - \frac{\lambda}{24}\bar{\Phi}^4 - \varphi\left(m^2\bar{\Phi} + \frac{\lambda}{6}\bar{\Phi}^3\right) + \frac{1}{2}\varphi(-d^2 - m^2)\varphi - \frac{\lambda}{4}\bar{\Phi}^2\varphi^2 - \frac{\lambda}{6}\bar{\Phi}\varphi^3 - \frac{\lambda}{24}\varphi^4. \tag{16}$$

To lowest order (Hartree approximation) we substitute the fluctuations by their expectation values. Using the fact that $\langle\varphi\rangle = 0$ we find up to a constant

$$\mathcal{L} = -\frac{1}{2}\left(m^2 + \frac{\lambda}{2}\langle\varphi^2\rangle\right)\bar{\Phi}^2 - \frac{\lambda}{24}\bar{\Phi}^4. \tag{17}$$

This means that the effective mass is modified by the effect of the fluctuations. Since the mass dimension of the field is $[\varphi] = 1/2$, by dimensional reasons $\langle\varphi^2\rangle \sim T$. On the other hand this is a correction to the mass squared, and so the coefficient is also dimensionful, and with finite lattice

spacing it is proportional to a^{-1}. The coefficient in leading order in perturbation theory reads

$$\langle\varphi^2\rangle = \frac{T}{N^3}\sum_{k\in\tilde{U}}\frac{1}{\sum_{i=1}^{3}4\sin^2(\frac{\pi k_i}{N})+m^2} \overset{N\to\infty}{\to} 0.2527T - \frac{mT}{4\pi} + \mathcal{O}(m^2), \tag{18}$$

but this number is unreliable for large couplings.

One consequence of this formula is that at fixed negative bare mass the effective mass term will be positive at high enough temperature. This means that the minimum of the effective action for the constant field (the constrained free energy) will become zero at this temperature: the symmetry is restored. To see it we measured the expectation value of the field for various tree level masses at different temperatures. The result can be seen in Fig. 4.

A more delicate question is that in the 3D classical field theory, unlike in the four-dimensional theory, the temperature influences the renormalization. This means that the meaning of mass and temperature cannot be separated from each other in that clear way as it can be done in the 4D case. We therefore also performed simulations with fixed effective mass at different temperatures: this requires us to tune the bare mass parameter. In practice we fix the desired effective mass and the bare mass, and tune the temperature accordingly with the application of Langevin equations described earlier.

For the definition of the mass we measured the correlation function

$$G(t,\mathbf{x}) \coloneqq \langle\Phi(t,\mathbf{x})\Phi(0)\rangle. \tag{19}$$

In the leading order of perturbation theory, we expect that this correlator is the free one, where we should also take into account the mass modification:

$$G(t,\mathbf{k}) = \langle|\Phi_k|^2\rangle\cos\omega_k t, \tag{20}$$

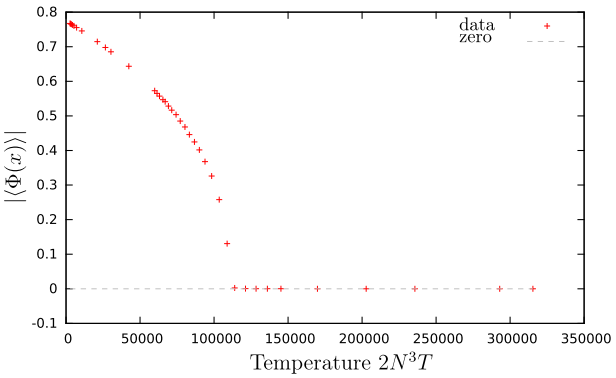

FIG. 4 (color online). Temperature dependence of the expectation value of the field.

where $\omega_k^2 = \mathbf{k}^2 + m^2 + \frac{\lambda}{2}\langle\varphi^2\rangle$. If one goes beyond the first order of perturbation theory, then one obtains self-energy corrections, and the pure harmonic behavior of the correlator will be spoiled. If a one-particle mass shell is dominant, then we can speak about quasiparticle excitations. In that case in real time evolution one can observe a damped oscillation:

$$G(t,\mathbf{k}) \sim \exp(-t/\tau_k)\cos(\omega_k t). \tag{21}$$

However, the closer we are to the phase transition point, the worse behavior could be observed for the static Φ field, as it is demonstrated in Fig. 5. We can see that far from the phase transition point, where the effective mass is large, the quasiparticle assumption is valid. With decreasing effective mass, the fit works worse and worse. In this case the definition of the notion of "mass" is not unique anymore. For a more sophisticated description we should use the complete spectral function, but we just need a characterization of the mass and temperature. For that purpose we use the best quasiparticle fit to the real time data for the zero mode. This is some mean value of the spectral peak; in the vicinity of the phase transition point it remains finite, as opposed to the inverse spatial correlation length.

The temperature dependence of the mass defined by Eq. (21) is shown in Fig. 6 with fixed bare mass $m^2 = -0.5$. We can clearly see the position of the phase transition point which sits at the minimum of this curve. One may also check whether we reached the infinite volume (thermodynamical) limit. For that we determined the temperature dependence of the mass at various volumes; see the left panel of Fig. 7. This plot suggests that we have already reached the thermodynamical limit. We can also check the temperature dependence of the effective mass; this is shown in the right panel of Fig. 7. We see that for different bare masses, the effective mass values sit on a unique curve.

V. VISCOSITY

The central topic of this paper is the determination of the shear viscosity. The Kubo formula for momentum transport [1] requires us to compute

$$\eta = \lim_{\omega\to 0}\frac{\varrho_{T_{12}T_{21}}(\omega,\mathbf{k}=0)}{\omega}, \tag{22}$$

where

$$\varrho_{AB}(x) = \langle[A(x),B(0)]\rangle, \tag{23}$$

η is the shear-viscosity, and T_{12} is the one-two component of the energy momentum tensor; in the case of scalar field theory it is $T_{12} = \partial_1\Phi\partial_2\Phi$. In classical theory we cannot measure the commutator of two operators, but we can measure the correlation function instead. For the $A(x)$ and $B(0)$ operators it is defined as

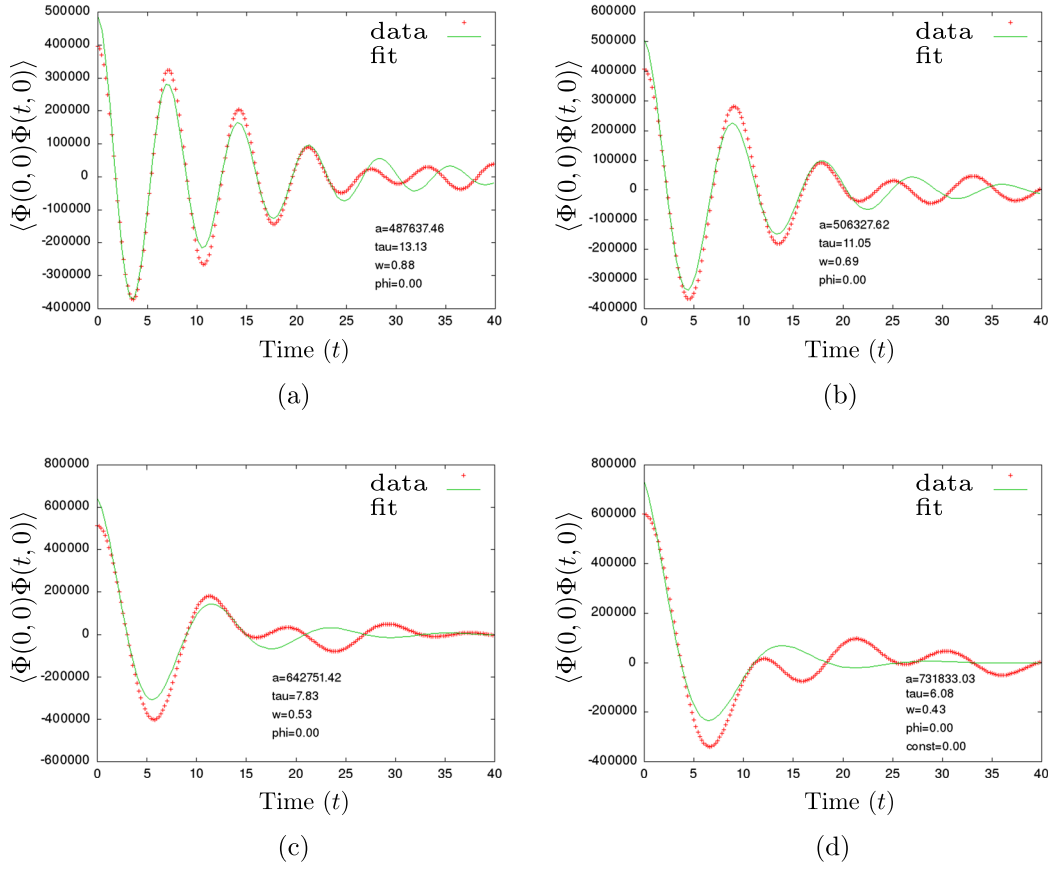

FIG. 5 (color online). The real time behavior of the field correlation function at different bare masses, $\lambda = 5$. (a) $M = 0.88$, (b) $M = 0.69$, (c) $M = 0.53$, and (d) $M = 0.43$.

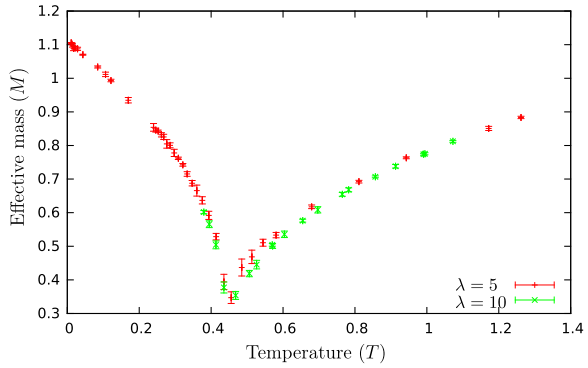

FIG. 6 (color online). Temperature dependence of the effective mass parameter for various interaction strength (λ) where $m^2 = -0.5$. It has a minimum at the phase transition point, but with our definition the minimum is not at zero.

$$S_{AB}(x) = \langle A(x)B(0)\rangle_{\rm cl}, \tag{24}$$

where the "cl" subscript refers to the classical correlation function. To connect this quantity with the viscosity we use the Green-Kubo formula, which claims that

$$\varrho_{AB,\rm cl}(\omega,\mathbf{k}) = \beta\omega S_{AB,\rm cl}(\omega,\mathbf{k}), \tag{25}$$

which is a direct consequence of the quantum Kubo-Martin-Schwinger relation

$$\varrho_{AB}(\omega,\mathbf{k}) = (1 - e^{-\beta\omega})S_{AB,\rm cl}(\omega,\mathbf{k}), \tag{26}$$

in the $\beta\omega \to 0$ limit. Using this relation the viscosity is

$$\eta_{\rm cl} = \beta S_{T_{12}T_{12}}(k = 0). \tag{27}$$

The direct result of our simulations in real time can be seen in Fig. 8. We repeated the measurements of $S_{T_{12}T_{12}}$ for five different configurations, meaning that after each measurement we allowed the system to evolve in time until we reached an independent configuration. This makes it possible to estimate the statistical error of the simulation.

The relevant information, the transport peak can be extracted from the Fourier-transformed data shown in Fig. 9. To understand what we see in this figure, we recall that in the leading order of perturbation theory we expect a branch cut starting at $2m$, and a Dirac-delta peak at $k = 0$, just like in the Fourier transform of $\langle\Phi^2(x)\Phi^2(0)\rangle$. The higher order terms result in the smearing of the cut and the Dirac-delta peak as well, the former yielding a broad bump

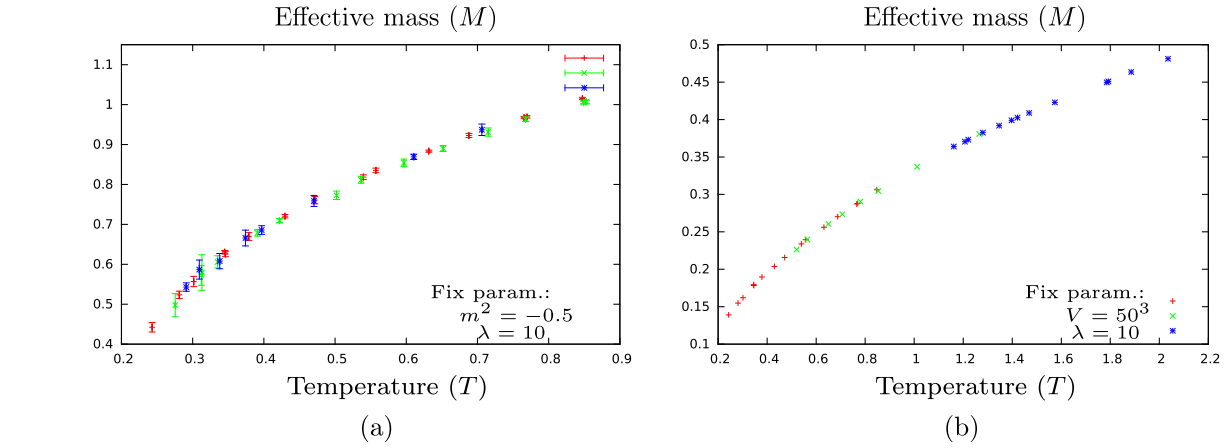

FIG. 7 (color online). Left panel: Effective mass at different volumes. Right panel: Effective mass in theories with different bare mass. (a) various volumes, (b) various Lagrangian m.

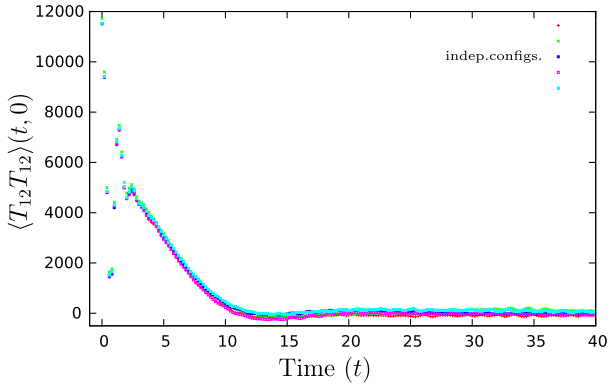

FIG. 8 (color online). T_{12} autocorrelation function in real time.

and the latter leading to the transport peak. The desired result is the height of this peak at $\omega = 0$.

One can repeat this measurement at different temperatures as well; this can be seen in Fig. 10. This figure suggests that the classical shear viscosity depends more or less linearly on the temperature. It also follows from dimensional analysis: since $[\Phi] = 1/2$ is the mass dimension of the field, $[T_{12}] \sim 3$, its correlator has 6th power of energy dimension. After Fourier transformation there remains 2, and after division by the temperature there remains 1, a linear energy dependence. Since the main source of energy dependence in the classical case is the temperature, we expect proportionality with T. From the very same line of thought in 4D one obtains the usual $\eta \sim T^3$ dependence (here $[\Phi]=1$, $[T_{12}]=4$, $[\langle T_{12}T_{12}\rangle] = 8$, in Fourier-space it has the dimension 4, and after division by the temperature there remains 3).

To numerically verify this, we also present the $\eta_{\rm cl}/T$ curve in Fig. 11. We see that the ratio is approximately constant, but with an enhanced behavior near the critical point. This figure suggests that the classical viscosity, just like other susceptibilities, shows a critical behavior, exhibiting a peak at the phase transition point.

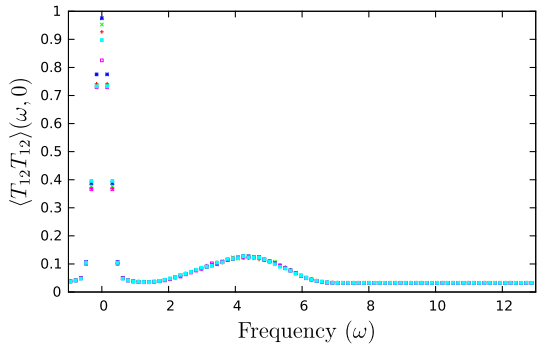

FIG. 9 (color online). T_{12} correlator in frequency space.

A. Interpretation

One can compute the classical viscosity in perturbation theory to leading order, similarly to what was done in Ref. [37]. With point splitting we can write

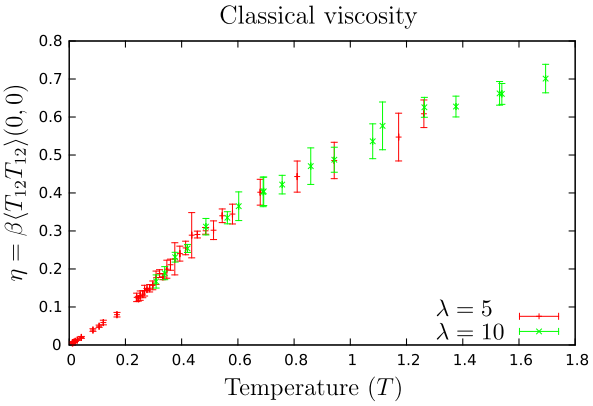

FIG. 10 (color online). Temperature dependence of the classical shear viscosity.

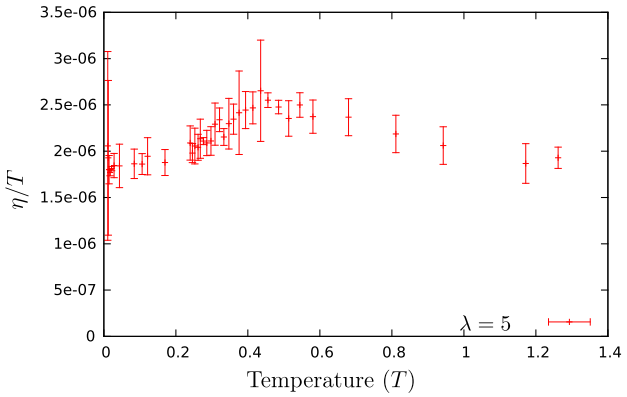

FIG. 11 (color online). Classical shear viscosity over temperature as a function of the temperature. The enhanced behavior is around the phase transition point, suggesting that the viscosity also shows a critical behavior.

$$\begin{aligned} S(x) &= \langle T_{12}(x)T_{12}(0)\rangle \\ &= \lim_{\substack{x'\to x \\ y'\to y\to 0}} \partial_{x1}\partial_{x'1}\partial_{y1}\partial_{y'1}\langle\Phi(x)\Phi(x')\Phi(y)\Phi(y')\rangle \\ &= \partial_1^2 iG_{3D}(x)\partial_2^2 iG_{3D}(x) + (\partial_1\partial_2 iG_{3D}(x))^2. \end{aligned} \tag{28}$$

After Fourier transformation we have

$$\begin{aligned} S(p) &= \int \frac{d^4k}{(2\pi)^4}[k_1^2(p-k)_2^2 + k_1k_2(p-k)_1(p-k)_2] \\ &\quad \times iG_{3D}(k)iG_{3D}(p-k) \\ &= T^2\int \frac{d^4k}{(2\pi)^2}\frac{k_1^2(p-k)_2^2 + k_1k_2(p-k)_1(p-k)_2}{k_0(p_0-k_0)} \\ &\quad \times \varrho(k)\varrho(p-k). \end{aligned} \tag{29}$$

This is very similar to the $\Phi^2\Phi^2$ correlation function discussed in [37], and also very similar to the discontinuity of the quantum version of it.

To proceed we use the Green-Kubo relation (27) to write

$$\eta_{\rm cl} = 2T\int \frac{d^4k}{(2\pi)^4}\frac{k_1^2k_2^2}{k_0^2}\varrho^2(k). \tag{30}$$

Evaluating this expression with the free spectral function (12) we obtain infinity: this means that for free theories the viscosity, like all other transport coefficient, is infinite. We can apply a Breit-Wigner approximation for the spectral function

$$\varrho(k) = \frac{4k_0\gamma_k}{(k_0^2-\omega_k)^2 + 4k_0^2\gamma_k^2}; \tag{31}$$

then we can approximate for small width and for $k_0 > 0$:

$$\varrho^2(k) \approx \frac{2\pi}{\gamma_k\omega_k^2}\delta(k_0-\omega_k). \tag{32}$$

This leads to

$$\eta_{\rm cl} = 4T\int \frac{d^3\mathbf{k}}{(2\pi)^3}\frac{k_1^2k_2^2}{\gamma_k\omega_k^4}. \tag{33}$$

This integral is still divergent in the continuum limit. The leading contribution comes from large momenta. The asymptotics of $\gamma_k\omega_k$ has been found in [37] (see also [24]); it is $\frac{\lambda^2T^2}{384\pi}$. In the remaining ω_k^{-3} factor, one can set $m = 0$. Therefore to leading order we have

$$\eta_{\rm cl} = \frac{1536\pi}{\lambda^2T}\int \frac{d^3\mathbf{k}}{(2\pi)^3}\frac{k_1^2k_2^2}{(k_1^2+k_2^2+k_3^2)^{3/2}} + \cdots \tag{34}$$

Rewriting this integral in terms of the dimensionless momenta ka and integrating it in the Brillouin zone $-\pi < ka < \pi$, one finds

$$\eta_{\rm cl} = \frac{\eta_{\rm lat}}{a^4}, \qquad \eta_{\rm lat} = \frac{321.3\pi}{\lambda^2T} + \cdots \tag{35}$$

The fact that $\eta_{\rm cl} \sim a^{-4}$ is consistent with the results of [37] for the Φ^2 autocorrelation function. There a logarithmic divergence was found; therefore the energy-momentum tensor correlation function, which has two derivatives more than Φ^2, should scale as a^{-4}.

Although this result is just a first order perturbative estimate, the robust part of the result is that the classical shear viscosity is proportional to a^{-4}. After determining $\eta_{\rm lat}$ by lattice simulations, this is the way one can recover the classical value of the viscosity.

The next question is how one can relate $\eta_{\rm cl}$ to the shear viscosity of quantum systems. The fact of the comparison of the classical and quantum calculations [37,40] was that the perturbative quantum result was rather close to the classical one, if one chooses a cutoff $\Lambda \sim T$. The exact value of the coefficient is not known to be universal; probably it depends on the quantity in question. But, up to a constant, we can estimate the result of the full quantum result by setting $\eta \sim (aT)^4\eta_{\rm cl}$. If we measure the shear viscosity from the lattice, we have

$$\eta \sim T^4\eta_{\rm lat}. \tag{36}$$

Below we will use unity for the proportionality constant.

Of course, this formula is based on the assumption that the quantum result is dominated by the classical fields. This may be true or not; it is out of the scope of the classical field theory study. *If* it is true, then our result has a significance. Also, unfortunately, we do not know the coefficient in this formula; nevertheless, we can give a temperature profile of the η/s ratio.

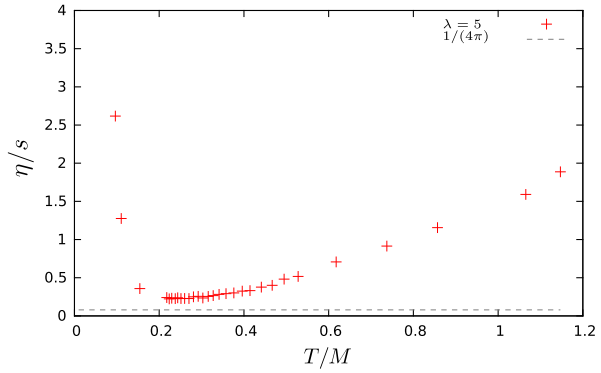

FIG. 12 (color online). The quantum η/s estimated by the classical Φ^4 theory, using $a = T^{-1}$ lattice spacing.

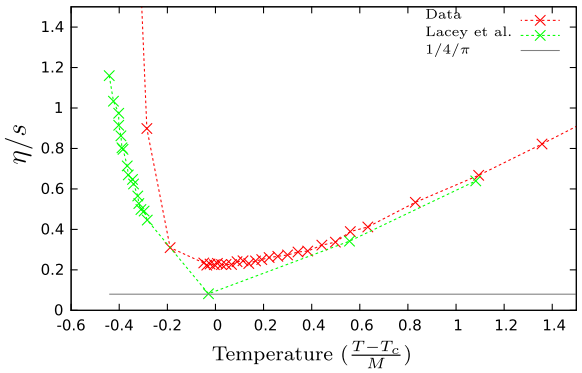

FIG. 13 (color online). Qualitative comparison of η/s of QCD plasma and the classical Φ^4 theory, after rescaling. The QCD data are taken from [41].

The entropy density of the quantum system is poorly approximated by the classical modes, so we use for the η/s estimate the entropy density of a free one-component gas with

$$s = \int \frac{d^3\mathbf{k}}{(2\pi)^3}\left[\frac{\omega_k}{e^{\beta\omega_k}-1} - \ln(1-e^{-\beta\omega_k})\right]. \tag{37}$$

Here $\omega_k^2 = \mathbf{k}^2 + m_{\text{eff}}^2$, where m_{eff} was taken from the classical simulations. In this way we can present our estimate for the η/s ratio in Fig. 12. We see a curve typical for the behavior of the shear viscosity in any matter near the phase transition point. For a qualitative comparison we show the η/s ratio for QCD [41] in Fig. 13 versus our results that was rescaled to fit to the high temperature part.

The characteristic form of the η/s ratio is not the consequence of the phase transition, present in the classical Φ^4 system, since, as we have seen in Figs. 10 and 11, this left the almost linear rise of the lattice entropy intact. More important is the behavior of the entropy density of a massive gas, which is exponentially suppressed at low temperatures, exhibits a fast rise, and later depends on the temperature as $\sim T^3$. The fast rise of the entropy is the reason behind the dip in the η/s curve.

VI. SUMMARY

In this work we used numerical simulations of the quartic classical field theory to give an estimate for the shear viscosity. To this end we solved the discretized classical equations of motion. This leads to thermalization, where one can determine the expectation value of different observables by time averaging. We first determined the field autocorrelation function, and analyzed it by assuming quasiparticle behavior. Then we measured the correlator of the one-two component of the energy-momentum tensor. Using the Green-Kubo formula this quantity is proportional to the shear viscosity. The shear viscosity η_{lat} was found to depend approximately linearly on T, which was expected by classical dimensional analysis. This behavior was superimposed by a characteristic critical behavior near the phase transition regime. Finally we pointed out that the classical viscosity comes from the lattice viscosity as $\eta_{\text{cl}} = \eta_{\text{lat}} a^{-4}$ where a is the lattice spacing. Translating the classical result into the shear viscosity of the quantum system, we argued that $a^{-1} \sim T$ is the correct choice, but the proportionality constant is not known. This allows us to make an estimate also on the temperature profile of η/s, which turns out to be rather similar to the result of QCD near the critical region.

As future prospects we plan to repeat this analysis to other models including gauge theories. Another interesting extension could be to study the effects of the quantum corrections to the equations of motion. This could provide a hint about the reliability of the classical estimate.

ACKNOWLEDGMENTS

The authors acknowledge useful discussions with A. Patkós and Zs. Szép. This research was supported by Grant No. K-104292 from the Hungarian Research Fund (OTKA).

[1] A. Hosoya, M. a. Sakagami, and M. Takao, Nonequilibrium thermodynamics in field theory: Transport coefficients, Ann. Phys. (N.Y.) **154**, 229 (1984).
[2] S. Jeon, Hydrodynamic transport coefficients in relativistic scalar field theory, Phys. Rev. D **52**, 3591 (1995).
[3] S. Jeon and L. G. Yaffe, From quantum field theory to hydrodynamics: Transport coefficients and effective kinetic theory, Phys. Rev. D **53**, 5799 (1996).
[4] A. Jakovac, Time evolution in linear response: Boltzmann equations and beyond, Phys. Rev. D **65**, 085029 (2002).
[5] P. B. Arnold, G. D. Moore, and L. G. Yaffe, Transport coefficients in high temperature gauge theories. 1. Leading log results, J. High Energy Phys. 11 (2000) 001.
[6] P. B. Arnold, G. D. Moore, and L. G. Yaffe, Transport coefficients in high temperature gauge theories. 2. Beyond leading log, J. High Energy Phys. 05 (2003) 051.
[7] A. Dobado and F. J. Llanes-Estrada, The viscosity of meson matter, Phys. Rev. D **69**, 116004 (2004).
[8] M. Buballa, K. Heckmann, and J. Wambach, Chiral restoration effects on the shear viscosity of a pion gas, Prog. Part. Nucl. Phys. **67**, 348 (2012).
[9] S. Mitra and S. Sarkar, Medium effects on the viscosities of a pion gas, Phys. Rev. D **87**, 094026 (2013).
[10] Z. Xu and C. Greiner, Thermalization of gluons in ultrarelativistic heavy ion collisions by including three-body interactions in a parton cascade, Phys. Rev. C **71**, 064901 (2005).
[11] Z. Xu and C. Greiner, Transport rates and momentum isotropization of gluon matter in ultrarelativistic heavy-ion collisions, Phys. Rev. C **76**, 024911 (2007).
[12] G. Aarts and J. M. Martinez Resco, Shear viscosity in the O(N) model, J. High Energy Phys. 02 (2004) 061.
[13] A. Peshier and W. Cassing, The Hot Non-Perturbative Gluon Plasma Is an Almost Ideal Colored Liquid, Phys. Rev. Lett. **94**, 172301 (2005).
[14] S. S. Adler *et al.* (PHENIX Collaboration), Elliptic Flow of Identified Hadrons in Au + Au Collisions at $s(NN)^{**}(1/2) =$ 200-GeV, Phys. Rev. Lett. **91**, 182301 (2003).
[15] J. Liao and V. Koch, On the fluidity and super-criticality of the QCD matter at RHIC, Phys. Rev. C **81**, 014902 (2010).
[16] H. B. Meyer, A calculation of the shear viscosity in SU(3) gluodynamics, Phys. Rev. D **76**, 101701 (2007).
[17] P. Petreczky, Progress in finite temperature lattice QCD, J. Phys. G **35**, 044033 (2008).
[18] P. Kovtun, D. T. Son, and A. O. Starinets, Holography and hydrodynamics: Diffusion on stretched horizons, J. High Energy Phys. 10 (2003) 064.
[19] P. Kovtun, D. T. Son, and A. O. Starinets, Viscosity in Strongly Interacting Quantum Field Theories from Black Hole Physics, Phys. Rev. Lett. **94**, 111601 (2005).
[20] G. Aarts and J. Smit, Finiteness of hot classical scalar field theory and the plasmon damping rate, Phys. Lett. B **393**, 395 (1997).
[21] B. J. Nauta and C. G. van Weert, Real time propagator for high temperature dimensional reduction, Phys. Lett. B **444**, 463 (1998).
[22] W. Buchmuller and A. Jakovac, Classical statistical mechanics and Landau damping, Phys. Lett. B **407**, 39 (1997).
[23] W. Buchmuller and A. Jakovac, Classical limit for scalar fields at high temperature, Nucl. Phys. **B521**, 219 (1998).
[24] G. Aarts and J. Berges, Classical Aspects of Quantum Fields Far from Equilibrium, Phys. Rev. Lett. **88**, 041603 (2002).
[25] B. Holdom, Approaching quantum behavior with classical fields, J. Phys. A **39**, 7485 (2006).
[26] J. Berges, S. Schlichting, and D. Sexty, Dynamic critical phenomena from spectral functions on the lattice, Nucl. Phys. **B832**, 228 (2010).
[27] T. Epelbaum, F. Gelis, and B. Wu, Nonrenormalizability of the classical statistical approximation, Phys. Rev. D **90**, 065029 (2014).
[28] S. Borsanyi, A. Patkos, and D. Sexty, Goldstone excitations from spinodal instability, Phys. Rev. D **66**, 025014 (2002).
[29] S. Borsanyi, A. Patkos, and D. Sexty, Nonequilibrium Goldstone phenomenon in tachyonic preheating, Phys. Rev. D **68**, 063512 (2003).
[30] D. Boyanovsky, C. Destri, and H. J. de Vega, The approach to thermalization in the classical φ^4 theory in $(1+1)$-dimensions: Energy cascades and universal scaling, Phys. Rev. D **69**, 045003 (2004).
[31] K. Dusling, T. Epelbaum, F. Gelis, and R. Venugopalan, Role of quantum fluctuations in a system with strong fields: Onset of hydrodynamical flow, Nucl. Phys. **A850**, 69 (2011).
[32] T. Epelbaum and F. Gelis, Role of quantum fluctuations in a system with strong fields: Spectral properties and thermalization, Nucl. Phys. **A872**, 210 (2011).
[33] J. Berges and D. Sexty, Bose Condensation Far from Equilibrium, Phys. Rev. Lett. **108**, 161601 (2012).
[34] K. Dusling, T. Epelbaum, F. Gelis, and R. Venugopalan, Initial state and thermalization, Nucl. Phys. **A910–911**, 437 (2013).
[35] J. Berges, K. Boguslavski, S. Schlichting, and R. Venugopalan, Basin of attraction for turbulent thermalization and the range of validity of classical-statistical simulations, J. High Energy Phys. 05 (2014) 054.
[36] J. Berges, B. Schenke, S. Schlichting, and R. Venugopalan, Turbulent thermalization process in high-energy heavy-ion collisions, Nucl. Phys. **A931**, 348 (2014).
[37] A. Jakovac, Viscosity of the scalar fields from the classical theory, Phys. Lett. B **446**, 203 (1999).
[38] M. Le Bellac, *Thermal Field Theory* (Cambridge University Press, Cambridge, England, 1996).
[39] http://www.fftw.org.
[40] E. k. Wang, U. W. Heinz, and X. f. Zhang, Spectral functions for composite fields and viscosity in hot scalar field theory, Phys. Rev. D **53**, 5978 (1996).
[41] R. A. Lacey, N. N. Ajitanand, J. M. Alexander, P. Chung, W. G. Holzmann, M. Issah, A. Taranenko, P. Danielewicz, and H. Stöcker, Has the QCD Critical Point Been Signaled by Observations at RHIC?, Phys. Rev. Lett. **98**, 092301 (2007).